Title

Cooperative Substrate Binding Controls Catalysis in Bacterial Cytochrome P450terp (CYP108A1).

Authors

Gable, Jessica
Poulos, Thomas
Follmer, Alec

Publication Date

2023-02-13

DOI

10.1021/jacs.2c12388

Peer reviewed

HHS Public Access

Author manuscript

J Am Chem Soc. Author manuscript; available in PMC 2024 August 13.

Cooperative Substrate Binding Controls Catalysis in Bacterial Cytochrome P450terp (CYP108A1)

Jessica A. Gable,
Departments of Chemistry, University of California, Irvine, Irvine, California 92697-3900, United States

Thomas L. Poulos,
Departments of Molecular Biology & Biochemistry, Departments of Pharmaceutical Sciences, and Departments of Chemistry, University of California, Irvine, Irvine, California 92697-3900, United States

Alec H. Follmer
Departments of Chemistry, University of California, Irvine, Irvine, California 92697-3900, United States

Abstract

Despite being one of the most well-studied aspects of cytochrome P450 chemistry, important questions remain regarding the nature and ubiquity of allosteric regulation of catalysis. The crystal structure of a bacterial P450, P450terp, in the presence of substrate reveals two binding sites, one above the heme in position for regioselective hydroxylation and another in the substrate access channel. Unlike many bacterial P450s, P450terp does not exhibit an open to closed conformational change when substrate binds; instead, P450terp uses the second substrate molecule to hold the first substrate molecule in position for catalysis. Spectral titrations clearly show that substrate binding to P450terp is cooperative with a Hill coefficient of 1.4 and is supported by isothermal titration calorimetry. The importance of the allosteric site was explored by a series of mutations that weaken the second site and that help hold the first substrate in position for proper catalysis. We further measured the coupling efficiency of both the wild-type (WT) enzyme and the mutant enzymes. While the WT enzyme exhibits 97% efficiency, each of the variants showed lower catalytic efficiency. Additionally, the variants show decreased spin shifts upon binding of substrate. These results are the first clear example of positive homotropic allostery in a class 1 bacterial P450 with its natural substrate. Combined with our recent results from P450cam showing complex substrate allostery and conformational dynamics, our present study with P450terp indicates that bacterial P450s may not be as simple as once thought and share complex substrate binding properties usually associated with only mammalian P450s.

Corresponding Author: **Alec H. Follmer** – *Departments of Chemistry, University of California, Irvine, Irvine, California 92697-3900, United States;* afollmer@uci.edu.

Supporting Information

The Supporting Information is available free of charge at https://pubs.acs.org/doi/10.1021/jacs.2c12388.
An account of crystallographic data collection and refinements, mutagenesis primers, additional UV–vis spectra, details of ITC, GC/MS, and NADH consumption analysis, and details for MD simulations and data (PDF)

Complete contact information is available at: https://pubs.acs.org/10.1021/jacs.2c12388

The authors declare no competing financial interest.

Graphical Abstract

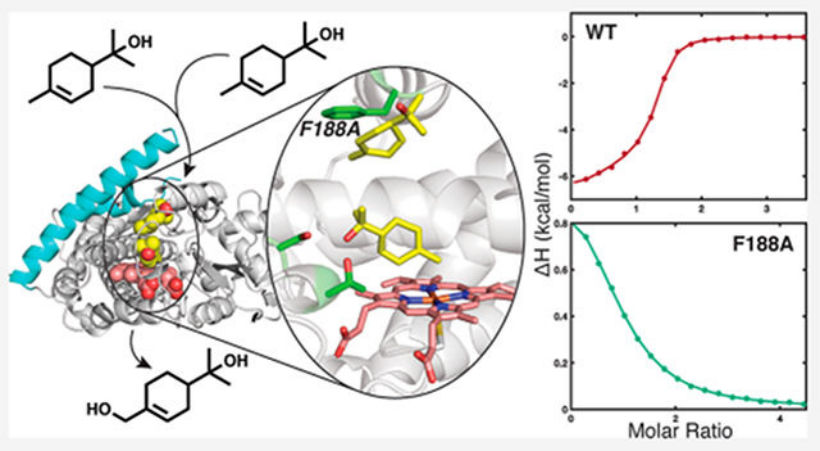

INTRODUCTION

Cytochromes P450 (CYPs or P450s) are heme-dependent monooxygenases that constitute one of nature's largest enzyme superfamilies and carry out critical metabolic reactions, including drug detoxification, steroid metabolism, natural product biosynthesis, and the oxidative assimilation of various organic compounds as carbon sources by some bacteria.[1] With such a broad functionality, P450s exhibit enormous sequence diversity.[2] Nevertheless, a conserved mechanism and a three-dimensional structure have allowed for structure–function relationships to be generalized across the superfamily. Critical to their chemistry, P450s employ a unique thiolate-ligated heme cofactor that generates highly oxidizing intermediates during the catalytic cycle such as ferryl-oxo/hydroxo ($Por^{\bullet+}$–Fe^{IV}=O/Por–Fe^{IV}–OH) species, compounds I and II, respectively.[3–5] While the catalytic cycle is well-studied, significantly less is known about the mechanisms by which these enzymes regulate the formation of their potent intermediates and prevent undesired oxidation of the protein scaffold.[6–8]

Despite these uncertainties, much more is known about the binding of substrate for the initiation of catalysis. Upon substrate binding, a change in the spin state is accompanied by an increase in the heme redox potential, allowing an electron to be transferred from a redox partner protein. This substrate-dependent control of the first electron transfer (ET) ensures that dioxygen binding to the reduced ferrous state only occurs when substrate is bound, minimizing the likelihood of unproductive dioxygen activation and generation of harmful radical oxygen species (ROS).[1]

Much of what we know about the molecular level details of P450s is derived from studies with *Pseudomonas putida* P450cam (CYP101A1), which was the first P450 to be sequenced[9,10] and have its crystal structure solved.[11] Like many other bacterial P450s, P450cam belongs to a class 1 system that requires two additional soluble ET proteins to perform catalysis. Specifically, a flavin adenine dinucleotide (FAD)-containing protein, putidaredoxin reductase (PdR), shuttles electrons from nicotinamide adenine dinucleotide

(NADH) to the Fe_2S_2 ferredoxin, putidaredoxin (Pdx), where the subsequent reduction of the heme iron by Pdx enables O_2 binding and activation followed by substrate hydroxylation. As more P450s were discovered and the number of detailed mechanistic studies expanded, it became clear that P450cam exhibits some additional unusual regulatory properties. The earliest unique feature of P450cam to be discovered was its strict requirement for its own redox partner,[12] while many other P450s can be supported by foreign redox partners.[13–16] We now know that Pdx binding to P450cam results in a Pdx-specific induced conformational change that triggers the formation of a proton relay network required for O_2 activation.[17–19] More recently, P450cam has been found to have a second allosteric substrate binding site and undergoes complex and large structural changes in response to the binding of heme iron ligands.[18,20]

Using P450cam as a model system, we find ourselves facing the important question: to what extent is the complexity of P450cam shared by other P450s? Given that P450cam is from *P. putida*, which uses camphor as a sole carbon source, we reasoned that other class 1*Pseudomonad* P450s that also use a terpenoid natural product as a sole carbon source might share similar properties. One example is P450terp (CYP108A1), a P450 that begins the oxidative assimilation of α-terpineol as a carbon source by hydroxylation, forming 7-hydroxy-terpineol (Scheme 1). P450terp is co-expressed with two ET proteins, an FAD-containing protein, terpredoxin reductase (TdR), and a Fe_2S_2 ferredoxin, terpredoxin (Tdx). CYP108A1 was the second *Pseudomonad* P450 to be characterized and have its crystal structure solved.[21–23] However, the available P450terp structure is substrate-free (SF), and enzymatic characterization is limited to a few publications.[24–28]

Here, we present the crystal structure of P450terp co-crystallized with its substrate, α-terpineol. Strikingly, this structure reveals two molecules of α-terpineol within the active site, which suggests that P450terp may exhibit homotropic allosteric control. We have explored this possibility with mutagenesis, additional crystal structures, molecular dynamics (MD) simulations, and substrate binding using both spectroscopic titration and isothermal titration calorimetry (ITC). These studies reveal that P450terp does indeed exhibit substrate cooperativity and that the allosteric site is required for efficient catalysis. Our results underscore how even the seemingly simplest cytochrome P450s can exhibit complex and diverse regulatory properties. Furthermore, we discuss these results in the context of the biological roles that these P450s serve in the metabolism of unusual alternative carbon sources.

METHODS

Protein Expression.

P450terp wild-type (WT) was encoded on a pET28a+ vector with an N-terminal His6-tag (Genscript). Primers for each mutation (Genewiz) were synthesized, and the variants with multiple mutations were created sequentially (i.e., WT to S101A, S101A/T103A, and S101A/T103A/F188A) (Table S2). Site-directed mutagenesis was performed using standard polymerase chain reaction (PCR) protocols (Takara PrimeSTAR Max). The vector was transformed into*E. coli* C41(DE3) cells and plated onto Luria broth (LB) plates containing 50 μg/mL kanamycin. Each mutation was verified by sequencing (Genewiz)

after performing minipreps (Macherey-Nagel) using standard protocols. Single colonies of each variant were taken to inoculate 100 mL of LB with 50 μg/mL kanamycin and grown overnight at 37 °C, 220 rotations per minute (rpm). The following day, 10 mL of the overnight starter culture was inoculated into 1 L of terrific broth (TB) supplemented with 50 μg/mL kanamycin. Cultures were grown at 37 °C and shaken at 220 rpm until OD_{600} = 0.8–1. Expression was induced with 1 mM isopropyl β-D-1-thiogalactopyranoside (IPTG) and supplemented with 0.4 mM 5-aminolevulinic acid (D-ALA). The temperature was then decreased to 25 °C. After 1 h, the speed was decreased to 100 rpm, and the cells were grown for 48 h, harvested, and then lysed or frozen.

Protein Purification.

Cells containing P450terp were resuspended in lysis buffer (50 mM KPi pH 7.4, 250 mM NaCl, and 2 mM β-mercaptoethanol, BME) and stirred overnight at 4 °C. Cells were lysed by two passes through a microfluidizer. The lysate was centrifuged for 1 h at 15,000 rpm at 4 °C (Beckman Coulter Avanti JA-17). The supernatant was loaded on to a nickel column pre-equilibrated with lysis buffer (Thermo Fisher HisPur Ni-NTA), washed with lysis buffer for 5 column volumes (CVs), and then washed with lysis buffer containing 15 mM imidazole for 5 CVs. The protein was eluted with lysis buffer containing 250 mM imidazole. Fractions exhibiting red color were collected, pooled, and dialyzed against wash buffer (50 mM KPi 7.4, 2 mM BME). Protein was removed from the dialysis bag and loaded on to a pre-equilibrated DEAE Sepharose column (Cytiva). The column was washed with 5 CVs of wash buffer followed by a gradient elution from 0 to 500 mM NaCl over the course of 10 CVs. Fractions with an optical purity ratio (Reinheitzahl, R/Z, A_{418}/A_{280}) of > 1.2 were pooled and dialyzed against wash buffer to remove salt. The protein was loaded on to a pre-equilibrated Q Sepharose column (Cytiva), washed, and eluted following the same steps as those for the DEAE column. Fractions displaying an R/Z of > 1.5 were pooled and concentrated to < 2 mL. The protein was loaded on to a pre-equilibrated size-exclusion chromatography (SEC) column (Cytiva Sephacryl S-200 HR) with SEC buffer (50 mM KPi pH 7.4, 150 mM NaCl, and 5 mM dithiothreitol, DTT). Fractions with R/Z > 1.8 were collected. Samples used for assays were buffer exchanged into 50 mM KPi pH 7.4 and 5 mM DTT in 30 kDa centrifugal filters (Millipore Amicon). Samples used for crystallization were buffer exchanged into 50 mM Bis-Tris pH 7.5 and 30 mM DTT in centrifugal filters.

Crystallization.

Crystals were grown from the Morpheus (MAKER) crystal screening condition (0.06 M magnesium chloride hexahydrate, 0.06 M calcium chloride dihydrate, 0.1 M sodium HEPES and MOPS pH 7.5, 20% v/v ethylene glycol, and 10% v/v PEG 8000) at 4 °C by hanging drop vapor diffusion. Hexagonal rods appeared within several days. SF crystals appeared bright red, while substrate-bound (SB) crystals appeared a darker reddish brown. SB crystals were grown in the same conditions, with the addition of the excess substrate in the mother liquor as well as the crystal drop. SF crystals grew significantly larger with the addition of 200 mM KCl in the mother liquor, while the same addition of KCl into the SB condition resulted in a loss of crystallization. Crystals used for X-ray diffraction were grown by sitting drop vapor diffusion (2 μL/2 μL, protein/condition). Mother liquor containing 25% glycerol was used as the cryoprotectant. Data were collected at the advanced light source

synchrotron (ALS). Data were indexed, integrated, and scaled using Mosflm and Scala.[29] Molecular replacement (MR) was performed using PHASER[30,31] by applying the SF P450terp (PDB:1CPT) as the MR model. Refinement was carried out in Phenix.refine[32,33] and COOT.[34,35] Refinement was further aided by PDB_REDO.[36] Data collection and refinement statistics are listed in Table S1.

Spectroscopy.

All ultraviolet–visible (UV–vis) spectroscopy characterizations were performed on a Cary 300 spectrophotometer. The following extinction coefficients were used: ε_{418} = 120 mM^{-1} cm^{-1} for SF P450terp WT and variants; ε_{396} = 96 mM^{-1} cm^{-1} for SB P450terp WT only; ε_{415} = 6.5 mM^{-1} cm^{-1} for Tdx; ε_{455} = 12.2 mM^{-1} cm^{-1} for TdR; and ε_{340} = 6.22 mM^{-1} cm^{-1} for NADH.[37]

Enzyme Assays.

The NADH consumption of the P450terp system was determined by monitoring the absorbance of NADH at 340 nm upon the addition of a substrate to a cuvette containing the catalytic components. The reconstituted systems contained 0.5 μM P450terp, 5 μM Tdx, 0.5 μM TdR, and 185 μM NADH in 50 mM KPi for a final volume of 980 μL. Reactions were initiated by the addition of 20 μL of 1 mM α-terpineol for a final volume of 1 mL and a concentration of 200 μM α-terpineol. Rates were determined using the least-squares regression method.

Isothermal Titration Calorimetry.

All experiments were performed on a MicroCal PEAQ-ITC instrument using a previously published protocol.[38] Concentrations of proteins and substrate were as follows: 100 μM P450terp WT in the cell and 2 mM α-terpineol in the syringe; 100 μM P450terp F188A in the cell and 2.5 mM α-terpineol in the syringe.

NADH/Substrate Coupling Assays.

Each coupling reaction was run in triplicate in microcentrifuge tubes (Thermo Fisher) at room temperature in 50 mM KPi pH 7.4, with the same protein concentrations as those for the spectral assays, and 122 μM α-terpineol. The reaction was initiated by adding 100 μM NADH. The reactions were given different end times to account for the different rates: 10 min for WT; 30 min for the S101A T103A and F188A variants; and >1 h for the S101A T013A F188A variant. Prior to extraction, an internal standard of camphor at 50 μM was added after the reactions were complete. Extraction was performed by adding 500 μL of dichloromethane (DCM) to the reaction mixture and vortexing for 30 s. The tubes were then centrifuged at 9000 rpm at room temperature for 5 min. The aqueous layer was removed, and the extraction procedure was repeated on the aqueous layer. Then, organic layers from both extractions were combined. The samples were run on a gas chromatography–mass spectrometry (GC–MS) system (Thermo Fisher), and data were analyzed in Chromeleon.

Computational Methods.

MD simulations were carried out using the GPU optimized *pmemd.cuda* in Amber 20.[39–41] Substrate parameters were assigned using the GAFF force field[42] and AM1-BCC charge scheme,[43,44] as implemented in the *antechamber* module in Amber. Heme parameters were taken from Shahrokh et al.[45] Our crystal structure of P450terp is missing residues 193–202. These were modeled in, and the geometry was optimized using Coot.[46] WT P450terp with either one or two substrate molecules bound was immersed in an octahedral box of water with a 10 Å cushion and neutralized with Na^+ ions. Initial structures of P450terp variants were prepared by alanine substitution of the WT structure in Pymol[47] and the same protocol as that used for the preparation of the WT structures. Structures were conjugate gradient minimized for 1000 cycles, allowing only H atoms and solvent molecules to move, followed by 10,000 cycles with no restraints. Solvent was allowed to relax using a constant volume heating from 5 to 300 K over 20 ps. This was followed with a 5 ns constant pressure simulation with protein backbone atoms restrained at 10 kcal $Å^{-2}$. Unrestrained production runs consisted of five separate 200 ns simulations starting with the same equilibrated structure but a different starting velocity. Snapshots were saved every 10 ps giving 20,000 frames for each 200 ns run. Trajectories were analyzed using *cpptraj* and *pytraj*.[48]

RESULTS

X-ray Crystallography.

We initially anticipated that P450terp would adopt a more closed conformation when the substrate binds given how commonly “open-to-closed” transitions are observed in other P450s.[1] As such, we co-crystallized P450terp in the presence of substrate rather than soaking α-terpineol into SF crystals to avoid restrictions of a conformational change by any restraints imposed by the crystal lattice. Regardless, the substrate–P450 complex crystallized with the same space group and cell dimensions as the previously determined SF structure (1CPT) and diffracted to a resolution of 2.0 Å.

Alignment of the SF and SB structures reveals a minimal change of the overall protein conformation with a Cα-RMSD of 0.26 Å between them (Figure S1A). In both structures, the loop connecting the F and G helices is disordered, but we were able to model a few more residues of the F–G loop than what was previously reported (Figure S1A). It was unclear whether this increase in ordered F–G loop density is due to the substrate binding, improved resolution, or advancements in data processing. We therefore also determined an α-terpineol-free P450terp structure to 2.0 Å, and both the SF and SB structures have the same number of F/G loop residues, which suggests that the newly ordered residues in our structure do not appear as a consequence of α-terpineol binding. However, the absence of substrate did not result in a vacant active site, but rather, a molecule of ethylene glycol provided by the mother liquor fits well into residual density above the heme (Figure S2).

Compared to P450cam, SB P450terp displays a more open active site due to the F–G loop disorder and positioning of the G-helix (Figure S1B), suggesting that P450terp may not undergo the open/close motions observed in other P450s. In P450cam, these motions change inter-residue couplings throughout the enzyme, which allows for the retention of

regioselectivity even upon an alteration of key interactions with the substrate.[49] It is then natural to question how P450terp positions α-terpineol for hydroxylation and maintains its regioselectivity. To our surprise, the SB structure exhibits two molecules of α-terpineol in the active site. A surface representation of the SB P450terp structure reveals two channels into the active site, each blocked by the second substrate (Figure S1C,D). While it is possible that disordered residues of the F–G loop cover the large channel between the two helices (Figure S1C), the number of unmodeled residues is insufficient to cover both channels simultaneously (Figure S1D).

Within the active site, electron density for the primary molecule of the substrate (terp1), the closest to the heme, is very well-defined and the carbon to be activated, C7, is positioned 4.2 Å from the heme iron (Figure 2A). In P450cam, the corresponding carbon atom of camphor, C5, is 4.0 Å from the iron.[11] The proximal substrate is held in place by key nonpolar contacts provided by Phe317 and Phe414 as well as hydrogen bonding interactions between the substrate hydroxyl group and the side chains of Ser101 and Thr103. Above terp1, large lobes of density were best modeled as a second substrate molecule (terp2) in two distinct but equally populated conformations refined to 49% and 51% occupancies (Figure 1C). Both conformations of terp2 clearly interact with the side chain of Phe188, with one conformation forming a hydrogen bond with the phenol sidechain of Tyr80. A Polder map of terp2 contoured at 5σ clearly shows the occupancy of a second molecule of the substrate and supports the existence of two conformations (Figure 1D). The closest distance between the two substrates is 4.0 Å, and there is minimal direct contact between the two molecules based on a space-filling model of the active site. The majority of the interaction between the two substrates is mediated by nonpolar contacts of the surrounding residues (Figure S3 and Table S4).

Guided by this structure and the hypothesis that the second substrate stabilizes the active site enabling efficient catalysis, we generated several active site mutants: a single mutant F188A to weaken the binding of the secondary molecule, a double mutant S101A/T103A to disrupt the primary, and a triple mutant S101A/T103A/F188A to perturb both sites. We were able to successfully co-crystallize and determine the structure of the single mutant F188A to 2.2 Å in the same conditions as those for the WT. While the Cα-RMSD between the WT and the F188A variant is 0.09 Å and terp1 remains similarly positioned within the active site, there is no electron density in the corresponding secondary site of F188A for the substrate or any other small molecule (Figure 2B). Additionally, albeit at a slightly lower resolution, the B-factor for terp1 in F188A also increases to 65.9 Å^2 from 35.2 Å^2 in the WT, consistent with the hypothesis that the second substrate molecule serves to stabilize the primary molecule for hydroxylation (Figure 2A). Upon reprocessing our WT structure at a lower, comparable resolution of 2.2 Å, the B-factor remains essentially unchanged at 35.3 Å^2, which supports our conclusion that the higher B-factor in the F188A structure results from the loss of the second α-terpineol.

Substrate Binding.

In the absence of α-terpineol, the UV–vis spectra of all four variants are nearly identical, displaying similar Soret maxima and Q-band profiles (Figure 3A). However, in the

presence of 1 mM α-terpineol (~300-fold excess), the variants show substantially different distributions of Soret intensities, corresponding to different populations of their nominal low- (418 nm) and high-spin (396 nm) states. The origin of the differences in the relative low-spin and high-spin populations is challenging to interpret and may be due to changes in the substrate dissociation constant, presence of an axial ligand, spin state equilibria, or some combination of these factors. As one may expect, the WT displays a complete shift to its respective high-spin species, similar to WT P450cam, indicating a complete occupation of the active site by α-terpineol. The single mutant F188A, which was designed to disrupt the secondary site, exhibits an incomplete shift, ~70% (Figure 3B), where even at high substrate concentrations (10 mM), the Soret does not fully interconvert to the SB spectrum (Figure S7). Since spectral changes of the Soret directly report on perturbations to the heme cofactor upon substrate binding, the decrease in the high-spin state formation reflects a decrease in the occupancy and/or greater mobility of the primary substrate position compared to that of the WT. Further, from the X-ray crystal structure, we know that mutation of Phe188 weakens the binding of α-terpineol in the second position, which in combination with the incomplete spin shift suggests that the binding ability of terp2 directly impacts the binding ability of terp1. The S101A/T103A variant displays a smaller Soret shift than the F188A mutant. Presumably, the elimination of hydrogen bonding interactions with the primary substrate molecule greatly decreases the affinity for the first site. Based on the crystal structure of SB WT P450terp, interactions with several hydrophobic residues nearby, Phe414 and Phe317, help retain some favorable interactions along with an unperturbed secondary site, which serves to entrap terp1 and leads to the observed partial spectral shift. As expected, the S101A/T103A/F188A variant displays the smallest high spin shift as critical contacts for both sites are eliminated (Figure 3C).

Another important point of comparison is the differences between the UV–vis absorption spectra of the different variants. The Soret maxima of WT and F188A remain identical at 418 nm in the absence of a substrate, while the variants containing S101A and T103A display shifted maxima at 419 and 421 nm in the double and triple mutants, respectively, indicating a change in their ground state electronic structure. Moreover, in the canonical carbon monoxide bound (CO-bound) P450 spectra, P450terp WT and the F188A variant exhibit P450-type spectra, while the S101A/T103A/F188A variant displays the “inactive” P420-type spectrum (Figure S14). In the presence of a substrate, the S101A/T103A variant is P450-type, and in the absence of a substrate, it is P420-type.

As the S101 and T103 residues are directly adjacent to the heme, it is likely that mutation of these residues does not only perturb substrate binding but also affects the stability, and therefore the electronic structure, of the heme. It seems that binding of the substrate in this case helps stabilize the heme pocket in the S101A/T103A variant. This is further evidenced upon examination of the spectra of the reduced species prior to CO binding, where the Soret of the S101A/T103A variant and triple mutant red-shifts to ~425 nm and the Q-bands are sharp and distinct from the broad profiles displayed by WT and F188A (Figure S14). Both the shift in the Soret as well as the sharp α and β bands at 528 and 560 nm, respectively, of the double and triple mutants are consistent with spectral features observed for pressure-inactivated ferrous P450 (P420) species as well as low-spin ferrous six-coordinate cytochromes c and b_5.[50–52] This similarity supports the assignment of the

reduced state of these P450terp variants as low-spin and/or hexacoordinate. It is also, therefore, interesting to note that these results are consistent with the previous work that demonstrates that a histidine ligand is not necessary for the formation of the “inactivated” P420 species.[53]

Binding Affinities of α-Terpineol.

To test the hypothesis that substrates act cooperatively in the P450terp active site, we measured the binding affinities of α-terpineol to WT and F188A by UV–vis spectral titrations and ITC. From the spectral titrations, we determined the spectral binding constant, K_S, to be 2.67 μM for WT and 36.1 μM for the F188A variant (Table 1). More importantly, however, the data for WT were not well represented by the one- or two-site binding models (eqs S1 and S2), which contain the underlying assumption that each site exhibits a fixed and invariant affinity. Double-reciprocal plots of the data made this inadequacy obvious as the substrate dependency of the WT was not linear and displayed an upward concavity (Figure S16). The data were instead best fit to a binding site model utilizing a Hill coefficient that accounts for cooperative interaction between multiple substrates (eq S3). The fit of WT P450terp exhibited a Hill coefficient of 1.41, where a value >1 indicates positive cooperativity, consistent with our hypothesis (Figure 4A). We note that the assumptions underlying the Hill coefficient equation are not the most microscopically accurate representation of the binding modes occurring here. However, comparison to the F188A spectral titration still provides semi-quantitative and significant insights, as data for the mutant fit well to a one binding site model: 36.1 μM with a Hill coefficient of 1.01, indicating a lack of cooperativity (Figure 4B). As previously mentioned, since spectral titrations report on the status of the heme environment, it is therefore reasonably assumed that the obtained binding affinity of 36.1 μM reflects the diminished affinity of α-terpineol for the primary binding site as the secondary binding site has likely been impaired.

Corroboration for these observations was obtained by ITC where the thermodynamic binding profiles lead to similar conclusions. The titration of WT P450terp with α-terpineol was enthalpically driven, indicated by the negative heats of enthalpy in the binding curve (Figure S8). This observation contrasts with homologous P450 systems investigated by our lab, such as P450cam[38] and CYP101D1,[54] that display entropically driven bindings of the substrate. Additionally, each titration exhibited an unusual slow recovery to equilibrium in comparison to that in the previous work. The data for WT were best fit to a two-site binding model with dissociation constants, K_D, of 1.19 and 31.2 μM and site occupancies of 1.18 and 0.931, respectively (Figure 4C and Table 1). Again, recognizing that the assumptions of a two-site model are inadequate for a precise description of the affinities for these sites, we also fit the data to a single binding site model, which provides similar results with a slightly higher error. This fit resulted in a K_D of 2.69 μM, which is consistent with our spectrally determined binding constant (2.67 μM).

ITC titrations were performed with the F188A variant, and the data became rather complicated. With a reduced affinity for the second site, it was observed that substrate binding becomes apparently entropically driven. Entropically driven binding modes are generally attributed to the desolvation of hydrophobic substrates as they enter the active site,

which is to be expected of terpenoid compounds like camphor and α-terpineol.[55] Alteration of the second site exposes features associated with the affinity of a weakened active site. However, complication in the data interpretation arises upon the inspection of the baseline recovery of the titration. The F188A variant displays an enthalpic slow recovery phase post-injection, similar to WT (Figure S9). This slow re-equilibration phase caused difficulty in peak integration and proper assignment of a baseline for the titration. Inclusion of this slow feature into the background results in a well-defined binding curve that is best fit to a single binding site model with a K_D of 33.6 μM (Figure 4D and Table 1), matching the K_S of 36.1 μM for F188A. The reasoning for this inclusion is based on the assumption about the mechanism of binding and the origin of the slow re-equilibration phase. We assume that binding to the primary site is observed as the positive feature followed by the enthalpic stabilization of the primary site upon a cooperatively enhanced affinity for a debilitated second site. Therefore, subtraction of this enthalpic contribution reveals a binding constant for the active site in accordance with a K_S that reports directly on interaction with heme.

Turnover and Coupling Efficiency.

The structural and spectral/thermodynamic binding studies demonstrated the existence and impact of the second substrate site on active site stabilization. It is therefore reasonable to ask whether there is any influence of the secondary molecule on turnover performance. As discussed in the Introduction section, class 1 P450 systems require the shuttling of electrons from a molecule of NADH to and between three independent soluble proteins for turnover. As the rate limiting step of P450 catalysis is the first ET,[56] NADH consumption assays provide an indirect but simple measure of the activity (Scheme 1). Further, the ratio of NADH molecules consumed to the amount of the product formed allows for the coupling efficiency to be determined and related to the rate of reactivity from the consumption assays. P450cam displays a rapid rate of NADH consumption, ≈1000 min^{-1}, and an exemplary coupling efficiency of near 95%.[38,57] Due to the nearly complete shift to high-spin upon camphor binding in P450cam, it is tempting to suggest a relationship between the degree of the high-spin shift and coupling efficiency of enzyme turnover. However, it is important to keep in mind that systems such as CYP101D1 display a similar NADH consumption rate and coupling efficiency but do not demonstrate a complete high-spin shift.[58]

P450terp WT has a high turnover rate of 670 min^{-1}, comparable to that of P450cam and CYP101D1.[58] The coupling efficiency of P450terp was determined by substrate depletion monitored by GC/MS, revealing that WT is also almost perfectly coupled at 96.9%, which may be expected as both P450cam and P450terp fulfill the same biological role. Additionally, as expected, the S101A/T103A/F188A variant exhibited a negligible activity of 0.193 min^{-1} and accordingly is nearly completely uncoupled at 3.7% (Table 2).

Intriguingly, both the S101A/T103A and F188A variants showed moderate rates of NADH consumption. However, interpretation of their rates is complicated as they do not exhibit simple zero-order kinetics, possibly indicating a change in the rate-limiting step (Figure S10). Due to the complexities of determining the origin of this change, we report the qualitative observation that both rates are slow compared to WT, and the S101A/T103A variant is faster than the F188A variant. The S101A/T103A variant displays a

coupling efficiency of 70.6%, while F188A remains 51.2% coupled. The increased coupling efficiency of S101A/T103A compared to that of F188A highlights the importance of the secondary binding site for not only substrate binding but also its catalytic efficiency.

Molecular Dynamics.

The substrate stability of P450terp was assessed by analysis of five 200 ns MD simulations (100,000 total frames) for each variant. Simulations were carried out for WT with both one and two substrates in the active site as well as for the three mutants bound to two molecules of α-terpineol. The stability of terp1 in the P450terp active site was evaluated by two distance metrics: the heme center-of-mass (COM) to the terp1 COM and the distance from Fe to the carbon (C7) of α-terpineol that is hydroxylated. In simulations of each variant, the distances between the heme and terp1 COMs are multimodal with a clear dominant mode of ~7 Å. The WT simulations containing two molecules exhibit a dominant mode centered at 6.75 Å as well as two shorter and longer modes with smaller populations at 4.9 and 8.6 Å, respectively.

When WT P450terp is simulated with only one molecule in the active site, the distribution of distances changes significantly. The shorter distance mode increases over an angstrom to 5.65 Å and grows in population, while the central dominant mode also moves to a longer distance of 6.95 Å and broadens. At longer distances, the distribution spreads out and exhibits no clear maximum. While the distributions of distances are multimodal, the median, mean, and standard deviations (stds) provide useful metrics for comparing substrate behaviors between the different variants (Table 3). For example, both the mean and median COM distances for terp1 increase in the WT with one substrate, F188A, and S101A/T103A simulations compared to those in the WT with both substrate molecules present, demonstrating the dynamic control terp1 mobility by the second substrate and F188A The mobility of terp1, as indicated by the standard deviation, is the highest in WT with a single substrate, further reflecting the importance of the second molecule in stabilizing the primary α-terpineol for hydroxylation. The same trend of increasing distance and standard deviation holds for the Fe–C7 distance distributions, where the std of the single substrate simulations is essentially double that of all other variants. Furthermore, only the Fe–C7 distance of the single substrate runs exhibits multimodal behavior with two peaks at 4.40 and 8.75 Å. This bimodal behavior coupled to the dominant peaks of increased broadness exemplifies the increased mobility of terp1 in the active site. Except for a slight elongation, the Fe–C7 metrics for all the mutants are relatively similar.

The heme to terp2 COM distance also shows multimodal behavior across all simulations with highly variable distributions often exhibiting two equally populated modes. WT with both molecules of α-terpineol bound exhibits the shortest dominant mode at 11.40 Å, a second less populated mode at 14.75 Å, and a small population at 20.40 Å. The F188A, S101A/T103A, and S101A/T103A/F188A mutants all exhibit their middle modes as dominant at increased distances of 13.20, 15.20, and 13.40 Å, respectively, as well as increased populations of their farthest modes at 14.75, 20.00, and 14.50 Å, respectively, compared to that of WT. It is interesting to note the similarity between the profiles of the WT and S101A/T103A mutant and between F188A and S101A/T103A/F188A. While WT

and the double mutant display three distinct distance profiles at roughly the same distances (~11.5, ~15.0, and ~20.2 Å), variants containing F188A also exhibit similar profiles, but the modes become highly merged with peaks at ~11.4, ~13.3, and ~14.50 Å, respectively.

In order to understand whether motions between the heme, terp1, and terp2 are correlated, we computed the dynamic cross-correlation coefficients between these residues across the WT simulations. The cross-correlation (or normalized covariance) is a measure of correlated motion between two residues, where a value of −1 indicates completely anticorrelated motion, 0 indicates no correlation, and 1 indicates completely correlated motion.[59] The heme–terp1 and terp1–terp2 motions show strong correlation with coefficients of 0.673 and 0.677, respectively. The heme–terp2 motions are less strongly correlated with a coefficient of 0.504.

DISCUSSION

The importance of allosteric interactions in the regulation of cytochromes P450 chemistry is well-recognized, although the types of cooperativities exhibited by these systems are P450- and substrate-dependent, complex, and far from well-understood.[6,7] In this study, we demonstrated how cytochrome P450terp (CYP108A1) simultaneously and cooperatively binds two molecules of its substrate, α-terpineol. This type of allostery demonstrated by P450terp where the binding of multiple copies of the same substrate enhances the relative affinities of one another is referred to as positive homotropic allostery. In particular, the direct interaction of both substrate molecules within the same active site reflects a special type of positive homotropic cooperativity that is common among several P450s.[6,7] Positive homotropy is often discussed in the context of the most abundant P450 in humans, CYP3A4, which exhibits an extremely broad substrate profile and is responsible for the majority of xenobiotic metabolism.[60] In fact, due to its critical biological role, much of what we know about allosteric interactions in P450s originates from studies of the CYP3A4 isoform.[52] However, CYP108A1 serves a very different biological function than CYP3A4 and represents the first class 1 bacterial P450, to our knowledge, displaying positive homotropic allostery with its natural substrate that mediates catalytic efficiency.

This type of regulation represents an important concept in P450s that serve the biological role of oxidative assimilation of unusual carbon sources for energy. Several bacterial P450s have been shown to act as the first step in the oxidative metabolism of their substrates as sole carbon sources including P450cam,[62,63] P450terp,[21,64] P450lin,[65,66] P450cin,[67] and others.[68,69] Regulation of biodegradative P450 activity has been shown at the organismal,[70] genetic,[71–73] and protein levels.[20,74] Bacterial P450s of this type represent important targets in the development of whole-cell and enzymatic biocatalysts.[75] Descriptions of the regulatory mechanisms like those presented here for P450terp are, therefore, critical not only for our understanding of regulatory mechanisms in the bacterial metabolism but also to design systems that perform desired oxidative biotransformations.

Despite cytochrome P450terp originating from a plasmid-borne class 1 *Pseudomonad* system like P450cam, it does not display many of the characteristic features associated with substrate binding, including a large rearrangement of the F/G helices from an “open” form

to “closed” form or a shift of the I-helix. Instead, P450terp utilizes its second molecule of substrate to confer stability to the α-terpineol proximal to the heme center. This lack of a global conformational change upon substrate binding puts P450terp into a special category. In fact, historically, it was debated whether this type of interaction truly constitutes allostery given the lack of a clear conformational change, but it was later shown that microscopic conformational changes (or subensembles) can describe this class of cooperative systems referred to as “nested allostery”.[54]

Using X-ray crystal structures along with spectral and thermodynamic titrations, we confirmed that this second binding site positively contributes to the cooperative binding of the primary substrate and stabilizes it for hydroxylation. Mutation of Phe188 decreased the affinity for the second site so drastically that only the proximal substrate molecule was observed in the X-ray crystal structure of the F188A mutant. This observation along with the reduction of the Hill coefficient to 1 indicated a loss of any positive cooperativity. Further, inversion of the ITC binding profile from an enthalpic binding mode to an entropic binding mode corroborated these findings and is consistent with previous studies on P450cam and its homologues that display single binding sites in X-ray structures. The excellent agreement of the K_D and K_S (~36 μM) for this variant supports the suggestion that these titrations are reporting the affinity for a weakened primary site adjacent to the heme. Moreover, the F188A variant not only affects the affinity of the substrate for P450terp but also alters the rate of substrate turnover and efficiency of coupling. Upon mutation of Phe188, the coupling efficiency decreases by nearly half to 51.2% and substantially slows the rate of turnover, possibly changing the nature of the rate-limiting step.

Despite their differences in the substrate scope and biological function, CYP3A4 exhibits an analogous critical phenylalanine at 213 to Phe188 of P450terp. Mutation of Phe213 results in significant changes to homotropic and heterotropic allosteric effects involving 3A4 substrates carbamazepine, progesterone, and α-naphthoflavone.[61] In fact, the general region of the F–F‰ loop, also known as substrate recognition site 2 (SRS-2), is key for the control of positive homo- and heterotropic interactions. In CYP3A4, mutations in SRS-2 have been found to alter the responsiveness to allosteric effectors, diminish the extent of homotropic allostery, and even change the regioselectivity of substrate hydroxylation.[7]

Binding of the proximal substrate in P450terp, on the other hand, is controlled not only by interactions with the second substrate residing in the upper part of the active site channel but also through hydrogen bonding with residues next to the heme center, Ser101 and T103. Mutation of these two positions to alanine residues resulted in a loss of measurable substrate binding affinity as ITC indicated no heat change upon titration of α-terpineol and spectral titrations were impeded by substrate solubility and the lack of binding saturation. Additionally, while WT P450terp exhibits a rapid turnover (670 min^{-1}) and is highly coupled (97%), removal of S101 and T103 side chains significantly diminishes both the rate of turnover and the extent of coupling (70.6%). The triple mutant, where both the primary and secondary sites are affected, exemplifies the critical nature of these residues as both turnover and coupling efficiency are essentially abolished. The UV–vis spectra of reduced and CO-bound S101A/T103A and S101A/T103A/F188A variants (Figure S14), however, indicate these mutations may serve not only to destabilize substrate binding but

also to change the electronic structure the heme cofactor. It is, therefore, possible that this is what gives rise to a decrease in the coupling efficiency and the complicated NADH consumption kinetics. Moreover, this observation may also explain, in part, the reduced spin shift observed upon the addition of α-terpineol in the S101A/T103A-containing variants. Changes in the heme electronic structure (e.g., perturbations to the Fe–S bond) induced by these mutations may alter the ability of these variants to achieve the high-spin state even upon the binding of the substrate. Regardless, the lack of thermal changes in ITC isotherms of the S101A/T103A titrations supports the conclusion that these mutations substantially reduce the affinity for α-terpineol in the terp1 position. This reduction in affinity could also be accompanied by a change in the identity of the hydroxylated product if the substrate is more mobile within the active site and capable of reorientation.

MD simulations of P450terp support these experimental results where removal of terp2 in the WT enzyme and mutation of Phe188 to alanine both loosen the active site and allow for greater mobility of terp1. While the hydroxylated carbon of α-terpineol (C7) remains the closest carbon to the heme iron (~4.5 Å) in most of the simulations, the distance distribution broadens when only one substrate is bound to the active site or when the F188A mutation is included (Figures S18–S20). Additionally, the single substrate simulations are the only runs displaying bimodal behavior of terp1 with maxima at 4.40 and 8.75 Å. Together, these simulations support the importance of terp2 in the stabilization of terp1, and further, the increased mobility due to mutation of S101, T103, and F188 is reflected by the increase in B-factors of the second molecule of α-terpineol in comparison to that of WT as well as of terp1 in WT simulations with the second substrate removed (Figure S17 and Table S5).

While there are many instances of positive homotropic allostery in P450s, most do not reflect cooperative interactions with a natural substrate. This led to the hypothesis that open active sites were associated with substrate promiscuity of xenobiotic metabolizing P450s. Here, however, P450terp is believed to serve the sole purpose of hydroxylating α-terpineol and initiating the process of oxidative assimilation of α-terpineol as an alternative carbon source by its host organism. In contrast to many P450s exhibiting similar biological functions, P450terp exists in its “open” form in the presence of its natural substrate. Additionally, the occupancy of the endogenous substrate in the second site directly impacts catalytic efficiency, which has not been observed before in a class 1 bacterial system. While P450terp serves the same function and displays similar efficiency to P450cam, it is unlike P450cam in several ways. It is possible that the strict regulatory elements of P450cam may represent more extreme forms of regulation, while other bacterial systems like P450terp may display less stringent requirements, acting as a bridge for understanding substrate binding between the model system and more flexible isoforms.

This work demonstrates that this phenomenon may be much more common than previously appreciated but hard to capture in some P450 systems due to the nature of regulatory requirements for active site rearrangement. For example, in the structure of the complex of P450cam bound to its redox partner, Pdx, a well-ordered second camphor molecule is observed in three of the four asymmetric units just above the normal substrate binding site (Figure 1B).[17] The occupation of the open active site access channel with a second molecule of camphor was suggested to confer stability to the structure while holding the

primary molecule in place for oxidation, and it is possible that the same is occurring here in P450terp, though without the requirement for its redox partner.

The second molecule enters the P450cam active site upon a Pdx-induced conformational change of the enzyme to a more open form. As a result, critical salt bridges between Asp251 on the I-helix and two residues on the F-helix/loop region, Arg186 and Lys178, are broken. The freeing of Asp251 is accompanied by a change in the rotomer conformation to a position that faces the active site. This switch allows for the formation and participation of Asp251 in a proton relay network required for the controlled delivery of protons to the Fe–O_2 unit for the activation and subsequent heterolytic cleavage of the O–O bond.[18,19,76] P450terp contains an analogous aspartate (Asp270) on the I helix followed by a conserved threonine (Thr271) also critical for oxygen activation in P450cam (Thr 251).[77,78] Like Asp251 in P450cam, Asp270 in P450terp appears to be tied up in a similar but possibly weaker salt bridge with F-helix residue Gln185 as well as Lys419, which reaches over from the β5 sheet. Both interactions, however, engage the same carboxylate oxygen atom of Asp270 leaving the remaining side chain oxygen to participate in interactions with water molecules (Figure S4). While this does not preclude a redox partner-induced change in conformation, it does suggest that P450terp may not require the same redox partner-initiated global rearrangements to be activated for catalysis.

CONCLUSIONS

We have solved a crystal structure of P450terp with the substrate bound, wherein two substrate sites were revealed. Mutagenesis of these two sites showed a striking difference in their relative affinities for α-terpineol. Furthermore, the variants verified critical residues for substrate binding, and each decreased their rates of NADH consumption as well as coupling efficiencies. Along with an X-ray crystal structure of the F188A variant and substrate titrations, the turnover assays showed that binding to the second site directly contributes to the efficiency of P450 catalysis. While the presence of a second substrate molecule and its effects on reactivity may be relatively common in mammalian P450s, the occurrence of this behavior in bacterial P450s with small active sites is rather surprising. This exploration raises the question of how commonly multiple molecules of the substrate are present in the active site during catalysis and whether redox partner binding can initiate binding of multiple molecules when conformation changes are involved. It is quite possible that the serendipitous capture of the second substrate in crystals might represent an underappreciated but important tool in the evolution of P450 regulatory mechanisms.

Supplementary Material

Refer to Web version on PubMed Central for supplementary material.

ACKNOWLEDGMENTS

The authors would like to thank the SSRL and ALS beamline staff for their support during remote X-ray diffraction data collection as well as the San Diego Supercomputing Center (SDSC) for the use of the Triton Shared Computing Cluster (TSCC). This work was supported by NIH grant GM57353 (TLP). A.H.F. acknowledges support from GM120349 (Andrew S. Borovik). We also wish to pay tribute to the late Professor Julian Peterson who first discovered and characterized P450terp.

REFERENCES

(1). Poulos TL Heme Enzyme Structure and Function. Chem. Rev 2014, 114, 3919–3962. [PubMed: 24400737]

(2). Nelson DRA World of Cytochrome P450s. Philos. Trans. R. Soc., B 2013, 368, 20120430.

(3). Yosca TH; Ledray AP; Ngo J; Green MT A New Look at the Role of Thiolate Ligation in Cytochrome P450. JBIC, J. Biol. Inorg. Chem 2017, 22, 209–220. [PubMed: 28091754]

(4). Rittle J; Green MT Cytochrome P450 Compound I: Capture, Characterization, and C-H Bond Activation Kinetics. Science 2010, 330, 933–937. [PubMed: 21071661]

(5). Yosca TH; Rittle J; Krest CM; Onderko EL; Silakov A; Calixto JC; Behan RK; Green MT Iron(IV)Hydroxide p K_a and the Role of Thiolate Ligation in C–H Bond Activation by Cytochrome P450. Science 2013, 342, 825–829. [PubMed: 24233717]

(6). Davydov DR; Halpert JR Allosteric P450 Mechanisms: Multiple Binding Sites, Multiple Conformers or Both? Expert Opin. Drug Metab. Toxicol 2008, 4, 1523–1535. [PubMed: 19040328]

(7). Hlavica P Challenges in Assignment of Allosteric Effects in Cytochrome P450-Catalyzed Substrate Oxidations to Structural Dynamics in the Hemoprotein Architecture. J. Inorg. Biochem 2017, 167, 100–115. [PubMed: 27919007]

(8). Denisov IG; Frank DJ; Sligar SG Cooperative Properties of Cytochromes P450. Pharmacol. Ther 2009, 124, 151–167. [PubMed: 19555717]

(9). Haniu M; Armes LG; Tanaka M; Yasunobu KT; Shastry BS; Wagner GC; Gunsalus IC The Primary Structure of the Monoxygenase Cytochrome P450CAM. Biochem. Biophys. Res. Commun 1982, 105, 889–894. [PubMed: 7092907]

(10). Unger BP; Gunsalus IC; Sligar SG Nucleotide Sequence of the Pseudomonas Putida Cytochrome P-450cam Gene and Its Expression in Escherichia Coli. J. Biol. Chem 1986, 261, 1158–1163. [PubMed: 3003058]

(11). Poulos TL; Finzel BC; Howard AJ High-Resolution Crystal Structure of Cytochrome P450cam. J. Mol. Biol 1987, 195, 687–700. [PubMed: 3656428]

(12). Lipscomb JD; Sligar SG; Namtvedt MJ; Gunsalus IC Autooxidation and Hydroxylation Reactions of Oxygenated Cytochrome P-450cam. J. Biol. Chem 1976, 251, 1116–1124. [PubMed: 2601]

(13). Hannemann F; Bichet A; Ewen KM; Bernhardt R Cytochrome P450 Systems—Biological Variations of Electron Transport Chains. Biochim. Biophys. Acta, Gen. Subj 2007, 1770, 330–344.

(14). Liu X; Li F; Sun T; Guo J; Zhang X; Zheng X; Du L; Zhang W; Ma L; Li S Three Pairs of Surrogate Redox Partners Comparison for Class I Cytochrome P450 Enzyme Activity Reconstitution. Commun. Biol 2022, 5, 791. [PubMed: 35933448]

(15). Mendes MV; Antón N; Martín JF; Aparicio JF Characterization of the Polyene Macrolide P450 Epoxidase from *Streptomyces natalensis* That Converts de-Epoxypimaricin into Pimaricin. Biochem. J 2005, 386, 57–62. [PubMed: 15228385]

(16). Sawada N; Sakaki T; Yoneda S; Kusudo T; Shinkyo R; Ohta M; Inouye K Conversion of Vitamin D3 to 1α,25-Dihydroxyvitamin D3 by Streptomyces Griseolus Cytochrome P450SU-1. Biochem. Biophys. Res. Commun 2004, 320, 156–164. [PubMed: 15207715]

(17). Tripathi S; Li H; Poulos TL Structural Basis for Effector Control and Redox Partner Recognition in Cytochrome P450. Science 2013, 340, 1227–1230. [PubMed: 23744947]

(18). Follmer AH; Tripathi S; Poulos TL Ligand and Redox Partner Binding Generates a New Conformational State in Cytochrome P450cam (CYP101A1). J. Am. Chem. Soc 2019, 141, 2678–2683. [PubMed: 30672701]

(19). Poulos TL; Follmer AH Updating the Paradigm: Redox Partner Binding and Conformational Dynamics in Cytochromes P450. Acc. Chem. Res 2022, 55, 373–380. [PubMed: 34965086]

(20). Follmer AH; Mahomed M; Goodin DB; Poulos TL Substrate-Dependent Allosteric Regulation in Cytochrome P450cam (CYP101A1). J. Am. Chem. Soc 2018, 140, 16222–16228. [PubMed: 30376314]

(21). Peterson JA; Lu JY; Geisselsoder J; Graham-Lorence S; Carmona C; Witney F; Lorence MC Cytochrome P-450terp. Isolation and Purification of the Protein and Cloning and Sequencing of Its Operon. J. Biol. Chem 1992, 267, 14193–14203. [PubMed: 1629218]

(22). Boddupalli SS; Hasemann CA; Ravichandran KG; Lu JY; Goldsmith EJ; Deisenhofer J; Peterson JA Crystallization and Preliminary X-Ray Diffraction Analysis of P450terp and the Hemoprotein Domain of P450BM-3, Enzymes Belonging to Two Distinct Classes of the Cytochrome P450 Superfamily. Proc. Natl. Acad. Sci 1992, 89, 5567–5571. [PubMed: 1608967]

(23). Hasemann CA; Ravichandran KG; Peterson JA; Deisenhofer J Crystal Structure and Refinement of Cytochrome P450terp at 2.3 Å Resolution. J. Mol. Biol 1994, 236, 1169–1185. [PubMed: 8120894]

(24). Tuck SF; Peterson JA; Ortiz de Montellano PR Active Site Topologies of Bacterial Cytochromes P450101 (P450cam), P450108 (P450terp), and P450102 (P450BM-3). In Situ Rearrangement of Their Phenyl-Iron Complexes. J. Biol. Chem 1992, 267, 5614–5620. [PubMed: 1544935]

(25). Fruetel JA; Mackman RL; Peterson JA; Ortiz de Montellano PR Relationship of Active Site Topology to Substrate Specificity for Cytochrome P450terp (CYP108). J. Biol. Chem 1994, 269, 28815–28821. [PubMed: 7961838]

(26). Sevrioukova IF; Peterson JA Reaction of Carbon-Monoxide and Molecular-Oxygen with P450terp (CYP108) and P450BM-3 (CYP102). Arch. Biochem. Biophys 1995, 317, 397–404. [PubMed: 7893155]

(27). Andersson LA; Peterson JA Active-Site Analysis of Ferric P450 Enzymes: Hydrogen-Bonding Effects on the Circular Dichroism Spectra. Biochem. Biophys. Res. Commun 1995, 211, 389–395. [PubMed: 7794248]

(28). Andersson LA; Johnson AK; Peterson JA Active Site Analysis of P450 Enzymes: Comparative Magnetic Circular Dichroism Spectroscopy. Arch. Biochem. Biophys 1997, 345, 79–87. [PubMed: 9281314]

(29). Battye TGG; Kontogiannis L; Johnson O; Powell HR; Leslie AGW iMOSFLM: a new graphical interface for diffraction-image processing withMOSFLM. Acta Crystallogr., Sect. D: Biol. Crystallogr 2011, 67, 271–281. [PubMed: 21460445]

(30). McCoy AJ Solving structures of protein complexes by molecular replacement with Phaser. Acta Crystallogr., Sect. D: Biol. Crystallogr 2007, 63, 32–41. [PubMed: 17164524]

(31). McCoy AJ; Grosse-Kunstleve RW; Adams PD; Winn MD; Storoni LC; Read RJ Phaser crystallographic software. J. Appl. Crystallogr 2007, 40, 658–674. [PubMed: 19461840]

(32). Adams PD; Afonine PV; Bunkóczi G; Chen VB; Echols N; Headd JJ; Hung L-W; Jain S; Kapral GJ; Grosse Kunstleve RW; McCoy AJ; Moriarty NW; Oeffner RD; Read RJ; Richardson DC; Richardson JS; Terwilliger TC; Zwart PH The Phenix Software for Automated Determination of Macro-molecular Structures. Methods 2011, 55, 94–106. [PubMed: 21821126]

(33). Echols N; Grosse-Kunstleve RW; Afonine PV; Bunkóczi G; Chen VB; Headd JJ; McCoy AJ; Moriarty NW; Read RJ; Richardson DC; Richardson JS; Terwilliger TC; Adams PD Graphical tools for macromolecular crystallography in PHENIX. J. Appl. Crystallogr 2012, 45, 581–586. [PubMed: 22675231]

(34). Emsley P; Cowtan K Coot: model-building tools for molecular graphics. Acta Crystallogr., Sect. D: Biol. Crystallogr 2004, 60, 2126–2132. [PubMed: 15572765]

(35). Emsley P; Lohkamp B; Scott WG; Cowtan K Features and Development of Coot. Acta Crystallogr., Sect. D: Biol. Crystallogr 2010, 66, 486–501. [PubMed: 20383002]

(36). Joosten RP; Long F; Murshudov GN; Perrakis A ThePDB_REDOserver for macromolecular structure model optimization. IUCrJ 2014, 1, 213–220.

(37). Follmer AH Cytochrome P450: Nature's Aircraft Carrier. Ph.D, University of California: Irvine, 2019. https://www.proquest.-com/dissertations-theses/cytochrome-p450-natures-aircraft-carrier/docview/2275957801/se-2?accountid=14509 (accessed 2022 11 07).

(38). Batabyal D; Richards LS; Poulos TL Effect of Redox Partner Binding on Cytochrome P450 Conformational Dynamics. J. Am. Chem. Soc 2017, 139, 13193–13199. [PubMed: 28823160]

(39). Le Grand S; Götz AW; Walker RC SPFP: Speed without compromise-A mixed precision model for GPU accelerated molecular dynamics simulations. Comput. Phys. Commun 2013, 184, 374–380.

(40). Lee T-S; Hu Y; Sherborne B; Guo Z; York DM Toward Fast and Accurate Binding Affinity Prediction with PmemdGTI: An Efficient Implementation of GPU-Accelerated Thermodynamic Integration. J. Chem. Theory Comput 2017, 13, 3077–3084. [PubMed: 28618232]

(41). Mermelstein DJ; Lin C; Nelson G; Kretsch R; McCammon JA; Walker RC Fast and Flexible Gpu Accelerated Binding Free Energy Calculations within the Amber Molecular Dynamics Package. J. Comput. Chem 2018, 39, 1354–1358. [PubMed: 29532496]

(42). Wang J; Wolf RM; Caldwell JW; Kollman PA; Case DA Development and Testing of a General Amber Force Field. J. Comput. Chem 2004, 25, 1157–1174. [PubMed: 15116359]

(43). Jakalian A; Bush BL; Jack DB; Bayly CI Fast, Efficient Generation of High-Quality Atomic Charges. AM1-BCC Model: I. Method. J. Comput. Chem 2000, 21, 132–146.

(44). Jakalian A; Jack DB; Bayly CI Fast, Efficient Generation of High-Quality Atomic Charges. AM1-BCC Model: II. Parameterization and Validation. J. Comput. Chem 2002, 23, 1623–1641. [PubMed: 12395429]

(45). Shahrokh K; Orendt A; Yost GS; Cheatham TE Quantum Mechanically Derived AMBER-Compatible Heme Parameters for Various States of the Cytochrome P450 Catalytic Cycle. J. Comput. Chem 2012, 33, 119–133. [PubMed: 21997754]

(46). Casañal A; Lohkamp B; Emsley P Current developments in Coot for macromolecular model building of Electron Cryo-microscopy and Crystallographic Data. Protein Sci 2020, 29, 1055–1064.

(47). Schrödinger LLC. The PyMOL Molecular Graphics System, version 1.8, 2015.

(48). Roe DR; Cheatham TE PTRAJ and CPPTRAJ: Software for Processing and Analysis of Molecular Dynamics Trajectory Data. J. Chem. Theory Comput 2013, 9, 3084–3095. [PubMed: 26583988]

(49). Alvarez G; Le T; Wong N; Echave J; Pochapsky TC; Asciutto EK Hydroxylation Regiochemistry Is Robust to Active Site Mutations in Cytochrome P450 $_{cam}$ (CYP101A1). Biochemistry 2022, 61, 1790–1800. [PubMed: 35960510]

(50). Wells AV; Li P; Champion PM; Martinis SA; Sligar SG Resonance Raman Investigations of Escherichia Coli-Expressed Pseudomonas Putida Cytochrome P450 and P420. Biochemistry 1992, 31, 4384–4393. [PubMed: 1581294]

(51). Remba RD; Champion PM; Fitchen DB; Chiang R; Hager LP Resonance Raman Investigations of Chloroperoxidase, Horseradish Peroxidase, and Cytochrome c Using Soret Band Laser Excitation. Biochemistry 1979, 18, 2280–2290. [PubMed: 36129]

(52). Sligar SG; Egeberg KD; Sage JT; Morikis D; Champion PM Alteration of Heme Axial Ligands by Site-Directed Mutagenesis: A Cytochrome Becomes a Catalytic Demethylase. J. Am. Chem. Soc 1987, 109, 7896–7897.

(53). Gable JA; Tripathi S; Poulos TL Structural Insights on the Conversion of Cytochrome P450 to P420. ACS Omega 2022, 7, 18481–18485. [PubMed: 35694512]

(54). Batabyal D; Poulos TL Effect of Redox Partner Binding on CYP101D1 Conformational Dynamics. J. Inorg. Biochem 2018, 183, 179–183. [PubMed: 29550100]

(55). Murarka VC; Batabyal D; Amaya JA; Sevrioukova IF; Poulos TL Unexpected Differences between Two Closely Related Bacterial P450 Camphor Monooxygenases. Biochemistry 2020, 59, 2743–2750. [PubMed: 32551522]

(56). Brewer CB; Peterson JA Single Turnover Kinetics of the Reaction between Oxycytochrome P-450cam and Reduced Putidaredoxin. J. Biol. Chem 1988, 263, 791–798. [PubMed: 2826462]

(57). Kadkhodayan S; Coulter ED; Maryniak DM; Bryson TA; Dawson JH Uncoupling Oxygen Transfer and Electron Transfer in the Oxygenation of Camphor Analogues by Cytochrome P450CAM. J. Biol. Chem 1995, 270, 28042–28048. [PubMed: 7499289]

(58). Batabyal D; Poulos TL Crystal Structures and Functional Characterization of Wild-Type CYP101D1 and Its Active Site Mutants. Biochemistry 2013, 52, 8898–8906. [PubMed: 24261604]

(59). Hünenberger PH; Mark AE; van Gunsteren WF Fluctuation and Cross-Correlation Analysis of Protein Motions Observed in Nanosecond Molecular Dynamics Simulations. J. Mol. Biol 1995, 252, 492–503. [PubMed: 7563068]

(60). Guengerich FP CYTOCHROME P-450 3A4: Regulation and Role in Drug Metabolism. Annu. Rev. Pharmacol. Toxicol 1999, 39, 1–17. [PubMed: 10331074]

(61). Denisov IG; Grinkova YV; Nandigrami P; Shekhar M; Tajkhorshid E; Sligar SG Allosteric Interactions in Human Cytochrome P450 CYP3A4: The Role of Phenylalanine 213. Biochemistry 2019, 58, 1411–1422. [PubMed: 30785734]

(62). Hedegaard J; Gunsalus IC Mixed Function Oxidation. J. Biol. Chem 1965, 240, 4038–4043. [PubMed: 4378858]

(63). Katagiri M; Ganguli BN; Gunsalus IC A Soluble Cytochrome P-450 Functional in Methylene Hydroxylation. J. Biol. Chem 1968, 243, 3543–3546. [PubMed: 4297783]

(64). Peterson JA; Lu J-Y [60] Bacterial Cytochromes P450: Isolation and Identification. Methods Enzymol. 1991, 206, 612–620. [PubMed: 1784244]

(65). Madyastha KM; Bhattacharyya PK; Vaidyanathan CS Metabolism of a Monoterpene Alcohol, Linalool, by a Soil Pseudomonad. Can. J. Microbiol 1977, 23, 230–239. [PubMed: 851909]

(66). Renganathan V; Madyastha KM Linalyl Acetate Is Metabolized by *Pseudomonas incognita* with the Acetoxy Group Intact. Appl. Environ. Microbiol 1983, 45, 6–15. [PubMed: 16346182]

(67). Hawkes DB; Adams GW; Burlingame AL; Ortiz de Montellano PR; De Voss JJ Cytochrome P450cin (CYP176A), Isolation, Expression, and Characterization. J. Biol. Chem 2002, 277, 27725–27732. [PubMed: 12016226]

(68). Frank DJ; Waddling CA; La M; Ortiz de Montellano PR Cytochrome P450 125A4, the Third Cholesterol C-26 Hydroxylase from *Mycobacterium Smegmatis*. Biochemistry 2015, 54, 6909–6916. [PubMed: 26522442]

(69). Ikatsu H; Kino Y; Kawahara N; Adachi M, Miyoshi S-I; Tomochika K-I; Shinoda S Isolation and Characterization of Cytochrome P450-Producing Bacteria from Various Environments. Biocontrol Sci. 2000, 5, 111–116.

(70). Balaraman P; Plettner E Chemotaxis by Pseudomonas Putida (ATCC 17453) towards Camphor Involves Cytochrome P450cam (CYP101A1). Biochim. Biophys. Acta, Gen. Subj 2019, 1863, 304–312. [PubMed: 30391161]

(71). Fujita M; Aramaki H; Horiuchi T; Amemura A Transcription of the Cam Operon and CamR Genes in Pseudomonas Putida PpG1. J. Bacteriol 1993, 175, 6953–6958. [PubMed: 7693653]

(72). Aramaki H; Sagara Y; Hosoi M; Horiuchi T Evidence for Autoregulation of CamR, Which Encodes a Repressor for the Cytochrome P-450cam Hydroxylase Operon on the Pseudomonas Putida CAM Plasmid. J. Bacteriol 1993, 175, 7828–7833. [PubMed: 8253671]

(73). Subramanian V; Yadav JS Regulation and Heterologous Expression of P450 Enzyme System Components of the White Rot Fungus Phanerochaete Chrysosporium. Enzyme Microb. Technol 2008, 43, 205–213. [PubMed: 19730708]

(74). Skinner SP; Follmer AH; Ubbink M; Poulos TL, Houwing-Duistermaat JJ; Paci E Partial Opening of Cytochrome P450cam (CYP101A1) Is Driven by Allostery and Putidaredoxin Binding. Biochemistry 2021, 60, 2932–2942. [PubMed: 34519197]

(75). Cryle MJ; Stok JE; De Voss JJ Reactions Catalyzed by Bacterial Cytochromes P450. Aust. J. Chem 2003, 56, 749.

(76). Amaya JA; Batabyal D; Poulos TL Proton Relay Network in the Bacterial P450s: CYP101A1 and CYP101D1. Biochemistry 2020, 59, 2896–2902. [PubMed: 32574066]

(77). Martinis SA; Atkins WM; Stayton PS; Sligar SG A Conserved Residue of Cytochrome P-450 Is Involved in Heme-Oxygen Stability and Activation. J. Am. Chem. Soc 1989, 111, 9252–9253.

(78). Gerber NC; Sligar SG A Role for Asp-251 in Cytochrome P-450cam Oxygen Activation. J. Biol. Chem 1994, 269, 4260–4266. [PubMed: 8307990]

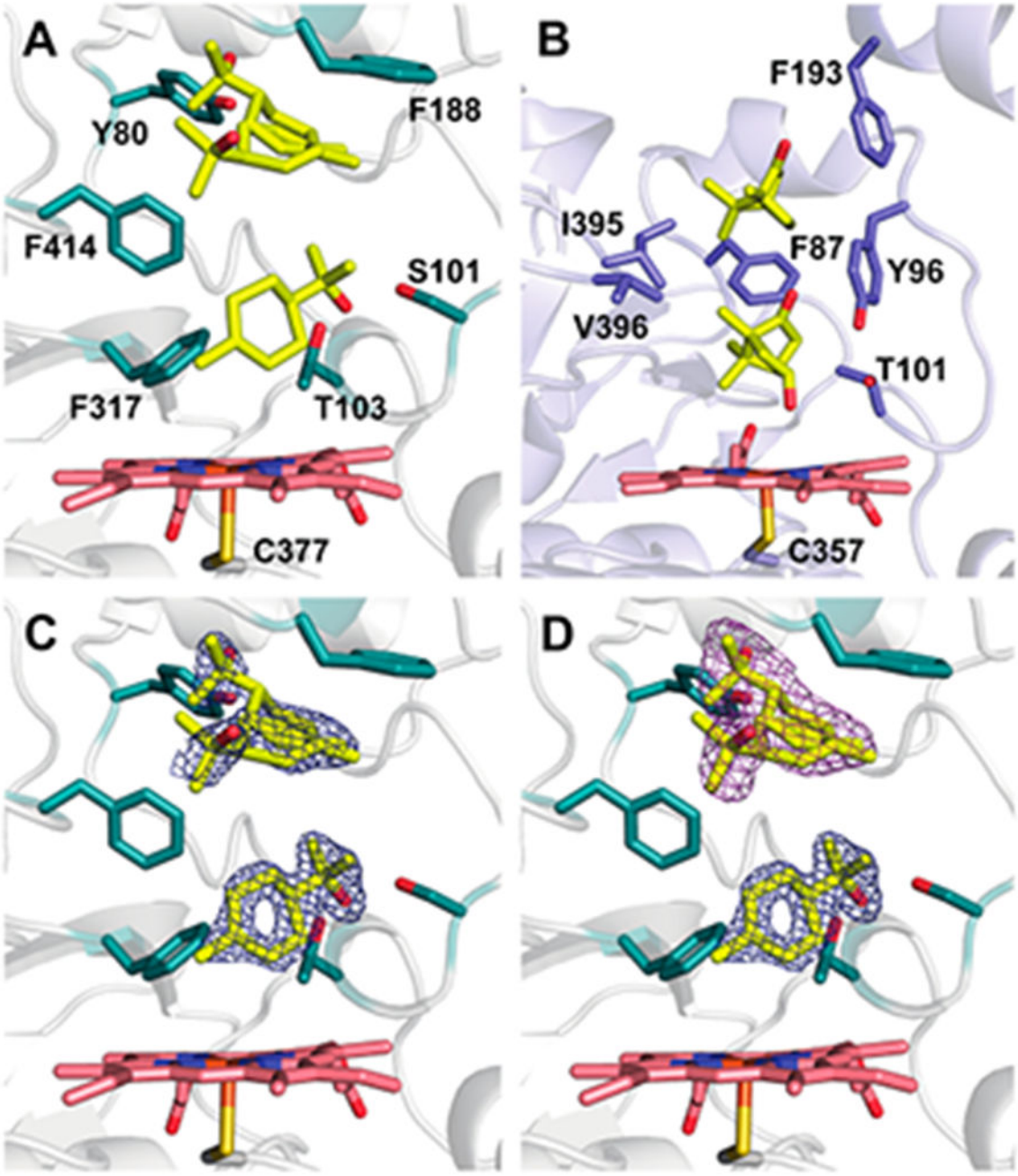

Figure 1.

Comparison of two molecules in active sites. (A) Two molecules of α-terpineol are bound in our crystal structure of P450terp. Residues contacting these molecules are shown. The bottom substrate (terp1) has one conformation, while the top substrate (terp2) has two alternate conformations. (B) Active site of P450cam in complex with Pdx is shown with one molecule of the product, 5-*exo*-hydroxycamphor, in the active site, and one molecule of the substrate, camphor, above it. The residues contacting these molecules are shown. (C) Electron density for the two molecules of α-terpineol is shown at 2σ for terp1 and 1σ for

terp2 of a $2F_O$-F_C map. (D) Polder map for the second substrate is shown in dark purple at 5σ.

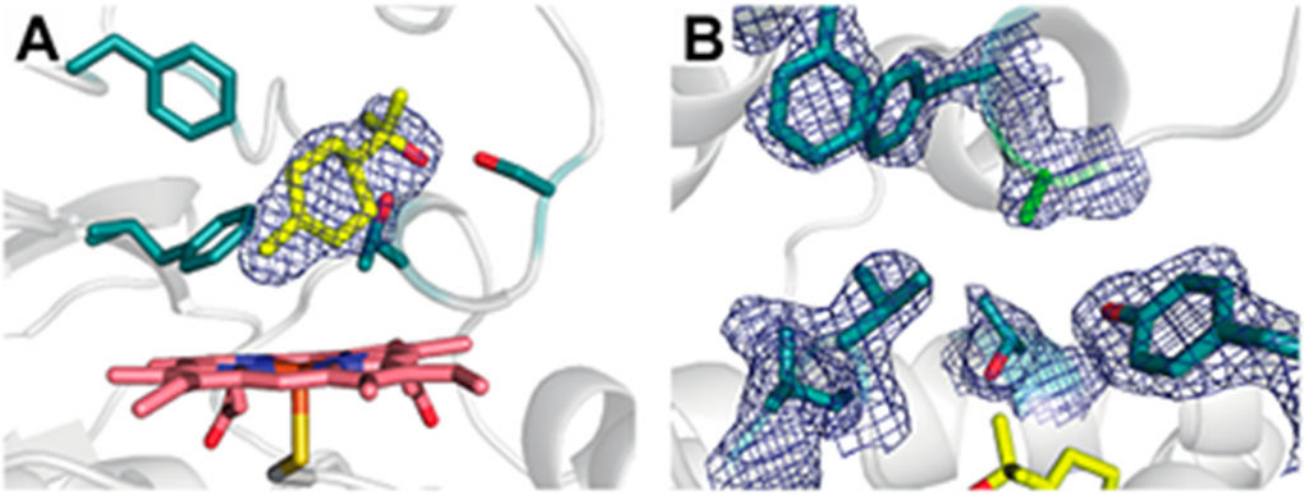

Figure 2.

Crystal structure of P450terp F188A. (A) Electron density for terp1 is shown at 1 < of a $2F_O-F_C$ map. (B) The second substrate site is shown with electron density at 1 <. The mutation of Phe188 to Ala is shown in green. No density is observed in the second site.

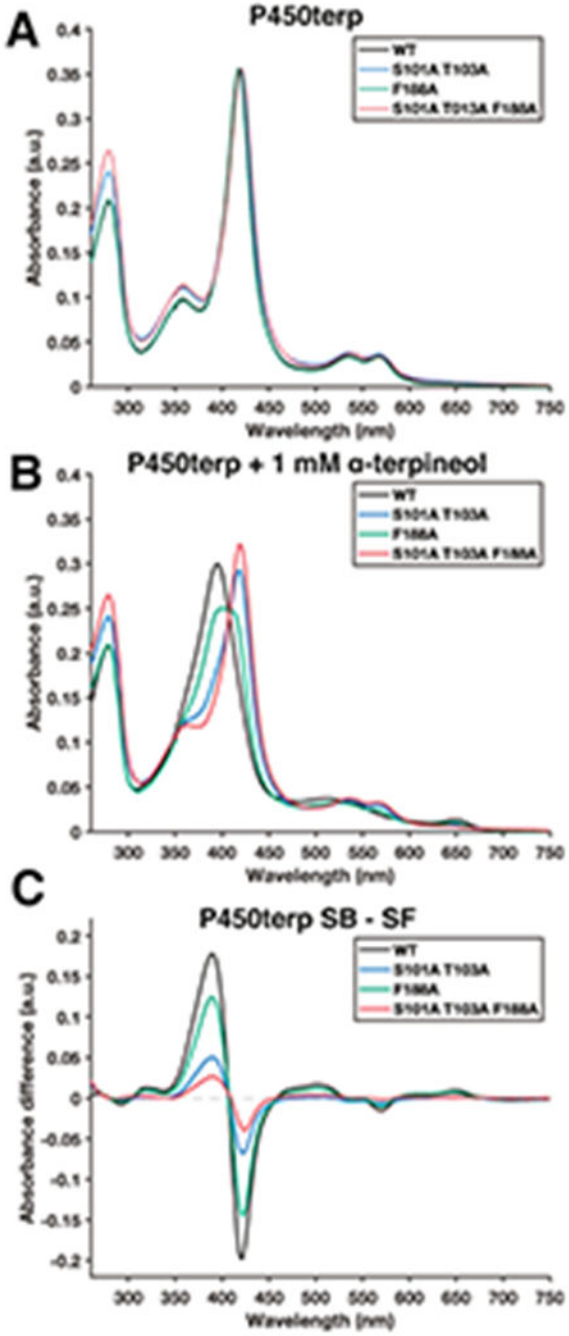

Figure 3.

Absorbance spectra of P450terp variants in the (A) absence and (B) presence of 1 mM α-terpineol in 50 mM KPi pH 7.4. (C) Substrate free (SF) subtracted from substrate bound (SB) difference spectra of P450terp variants.

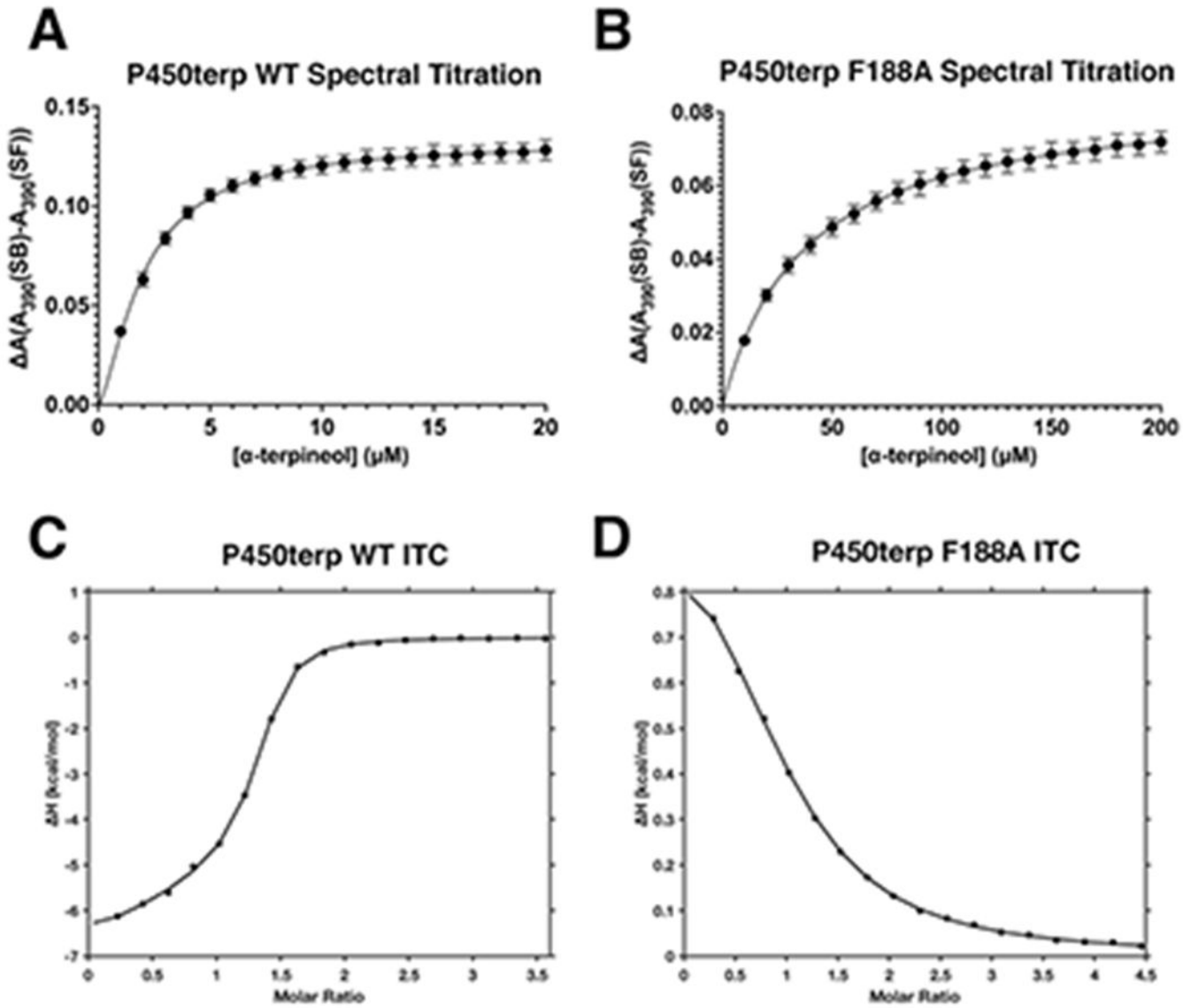

Figure 4.

Titration fittings for P450terp WT and the F188A variant. (A) Spectral titration of α-terpineol into P450terp WT fit to a single binding site with a Hill coefficient. (B) Spectral titration of α-terpineol into P450terp F188A fit to a single binding site. (C) ITC fit of α-terpineol into P450terp WT with a two-site binding model. (D) ITC fit of α-terpineol into P450terp F188A with a one-site binding model.

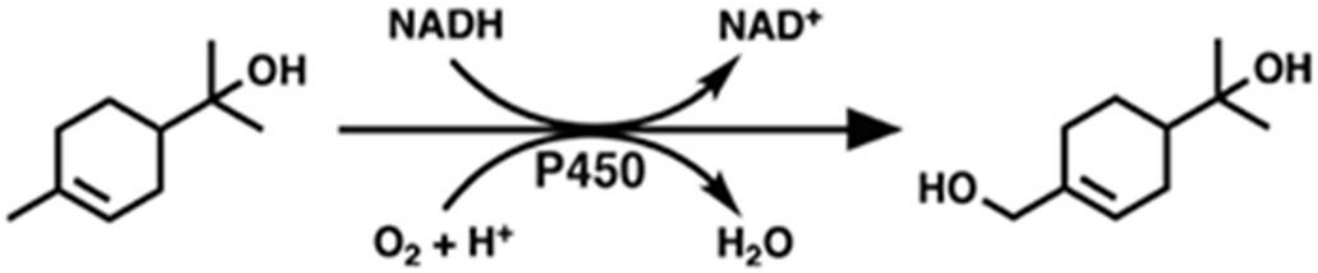

Scheme 1.

Net Reaction of the P450terp System[a]

[a]The FAD-containing TdR shuttles electrons from NADH to the Fe_2S_2-containing Tdx. Electrons are then transferred from Tdx to heme iron of P450terp for O_2 activation and hydroxylation of α-terpineol.

Table 1.

Binding Affinities of P450terp WT and F188A for α-Terpineol

P450terp	K_S (μM)	Hill coefficient	K_{D1} (μM)	N_1 (sites)	K_{D2} (μM)	N_2 (sites)
WT	2.67 ± 0.18	1.41	1.19 ± 0.09	1.18 ± 0.06	31.2 ± 3.7	0.931 ± 0.075
F188A	36.1 ± 1.4	1.01	33.6 ± 4.1	0.941 ± 0.011		

Table 2.

NADH Turnover Rates and Coupling Efficiency for P450terp Variants[a]

P450terp	NADH turnover (min^{-1})	coupling efficiency (%)
WT	676 ± 27	97 ± 1
S101A T103A		71 ± 1
F188A		51 ± 1
S101A T103A F188A	0.193 ± 0.045	3.7 ± 1.1

[a]The S101A T103A and F188A variants display complicated kinetics for NADH consumption, so their rates are not reported. Examples of these kinetics can be found in Figure S10.

Table 3.

Distance Metrics from MD Simulations of P450terp Variants[a]

P450terp		heme–terp1 (A)	Fe–C7 (A)	heme–terp2 (Å)
WT	mean	6.68 (0.85)	4.61(0.54)	14.25 (2.53)
	median	6.73	4.54	14.35
	peaks	[4.90, 6.75, 8.60]	4.40	[11.40, 14.75, 20.40]
WT–OS*	mean	6.94 (1.05)	5.17 (1.32)	
	median	6.89	4.83	
	peaks	[5.65, 6.95]	[4.40, 8.75]	
F188A	mean	6.62 (0.76)	4.88 (0.71)	14.01 (1.83)
	median	6.77	4.78	13.82
	peaks	[5.10, 6.90]	4.60	[11.35, 13.20, 14.75]
S101A T103A	mean	7.04 (0.57)	4.79 (0.59)	15.85 (2.62)
	median	6.98	4.71	15.48
	peaks	[6.95, 8.80]	4.65	[11.85, 15.20, 20.00]
S101A T103A F188A	mean	6.66 (0.76)	4.77 (0.65)	13.75 (1.51)
	median	6.74	4.70	13.80
	peaks	[5.80, 6.80]	4.60	[11.50, 13.40, 14.50]

[a]Standard deviations reported in the parentheses next to the associated mean.

*OS—one substrate.